Oxidative cyclizations in orthosomycin biosynthesis expand the known chemistry of an oxygenase superfamily

Kathryn M. McCulloch[a], Emilianne K. McCranie[b], Jarrod A. Smith[c], Maruf Sarwar[a], Jeannette L. Mathieu[a], Bryan L. Gitschlag[a], Yu Du[b], Brian O. Bachmann[b,c,1], and T. M. Iverson[a,c,1]

[a]Department of Pharmacology, Vanderbilt University, Nashville, TN 37232; [b]Department of Chemistry, Vanderbilt University, Nashville, TN 37235; and [c]Department of [c]Biochemistry, Vanderbilt University, Nashville, TN 37232

Edited by John T. Groves, Princeton University, Princeton, NJ, and approved July 2, 2015 (received for review January 26, 2015)

Orthosomycins are oligosaccharide antibiotics that include avilamycin, everninomicin, and hygromycin B and are hallmarked by a rigidifying interglycosidic spirocyclic ortho-δ-lactone (orthoester) linkage between at least one pair of carbohydrates. A subset of orthosomycins additionally contain a carbohydrate capped by a methylenedioxy bridge. The orthoester linkage is necessary for antibiotic activity but rarely observed in natural products. Orthoester linkage and methylenedioxy bridge biosynthesis require similar oxidative cyclizations adjacent to a sugar ring. We have identified a conserved group of nonheme iron, α-ketoglutarate–dependent oxygenases likely responsible for this chemistry. High-resolution crystal structures of the EvdO1 and EvdO2 oxygenases of everninomicin biosynthesis, the AviO1 oxygenase of avilamycin biosynthesis, and HygX of hygromycin B biosynthesis show how these enzymes accommodate large substrates, a challenge that requires a variation in metal coordination in HygX. Excitingly, the ternary complex of HygX with cosubstrate α-ketoglutarate and putative product hygromycin B identified an orientation of one glycosidic linkage of hygromycin B consistent with metal-catalyzed hydrogen atom abstraction from substrate. These structural results are complemented by gene disruption of the oxygenases *evdO1* and *evdMO1* from the everninomicin biosynthetic cluster, which demonstrate that functional oxygenase activity is critical for antibiotic production. Our data therefore support a role for these enzymes in the production of key features of the orthosomycin antibiotics.

antibiotic biosynthesis | oxidative cyclization | crystal structure | nonheme iron α-ketoglutarate–dependent oxygenases

Most currently available antibiotics are based upon one of a few scaffolds, with variants targeting the same biological process and having a common mechanism (1). However, bacterial resistance to structurally related compounds can occur rapidly and shorten the lifetime of a new antibiotic (2). Orthosomycins exhibit broad spectrum antibiotic properties against bacterial pathogens and hold therapeutic promise as they have a scaffold differing from other antibiotics and act on alternative targets. The orthosomycin everninomicin binds a unique site on the ribosome (3, 4) and is effective against resistant bacteria including methicillin resistant *Staphylococcus aureus* and vancomycin resistant enterococci (5). The everninomicin A congener (Ziracin) reached phase III clinical trials, but pharmacological complications prevented approval. However, everninomicin analogs or other natural congeners may still prove useful.

Produced by actinomycetes, orthosomycins are decorated oligosaccharides containing interglycosidic spirocyclic ortho-δ-lactone (orthoester) linkages, an uncommon functional group that enforces the interglycosidic angle necessary for antibiotic activity. The first orthosomycin described was hygromycin B (also called destomycin C), which was isolated from *Streptomyces hygroscopicus* in 1958 (6) and has one orthoester linkage (Fig. 1*A*, red). More complex orthosomycins include everninomicin and avilamycin, which each contain two orthoester linkages (Fig. 1*A*, red) and a methylenedioxy bridge (Fig. 1*A*, blue). Methylenedioxy bridge formation has previously been attributed to cytochrome P450 enzymes (7, 8). However, orthoester linkage biosynthesis has not previously been described. Orthoester linkage formation is associated with especially demanding steric constraints and substrates that are already highly oxygenated, and its biosynthesis results in a unique trioxaspiro functional group.

Everninomicin and avilamycin biosynthetic gene clusters encode upwards of 50 enzymes with many lacking assigned function. It has been suggested that within the avilamycin biosynthetic cluster in *Streptomyces viridochromogenes*, a set of putative α-ketoglutarate, nonheme iron-dependent [AKG/Fe(II)-dependent] oxygenases may be capable of catalyzing both orthoester linkage and methylenedioxy bridge formation (9, 10). AKG/Fe(II)-dependent oxygenases are powerful oxidants that catalyze a range of reactions, including oxidative cyclizations, hydroxylations, peroxidations, epoxidations, desaturations, and halogenations (11–14). This reactivity is suited to orthoester linkage and methylenedioxy bridge biosynthesis. However, practical challenges, including lack of knowledge of substrate identity and the difficulty in genetic manipulation of the producing organisms, have precluded validation of this prediction. We overcame these challenges by using the availability of closely related homologs (>70% identity) that synthesize different congeners of everninomicin and avilamycin. By combining our genomic and structural data (15), we propose that AKG/Fe(II)-dependent oxygenases can catalyze orthoester linkage formation.

Significance

Bacterial resistance to clinically relevant antibiotics has renewed public interest in identifying therapeutics with new scaffolds for the treatment of such infections. Analogs of orthosomycins could provide one such scaffold. One route to modifying these scaffolds is through rational engineering of the biosynthetic enzymes, requiring characterization of the biosynthetic pathway. A key feature of orthosomycin antibiotics is the orthoester linkage between carbohydrate groups, and our data suggest that a family of oxygenases is likely responsible for orthoester formation.

Author contributions: K.M.M., E.K.M., J.A.S., Y.D., B.O.B., and T.M.I. designed research; K.M.M., E.K.M., J.A.S., M.S., J.L.M., B.L.G., and Y.D. performed research; K.M.M., E.K.M., J.A.S., B.O.B., and T.M.I. analyzed data; and K.M.M., E.K.M., J.A.S., B.O.B., and T.M.I. wrote the paper.

The authors declare no conflict of interest.

This article is a PNAS Direct Submission.

Data deposition: The atomic coordinates and structure factors have been deposited in the Protein Data Bank, www.pdb.org (PDB ID codes 4XBZ, 4XAB, 4XAC, 4XAA, 4XC9, 4XCA, 4XCB, and 4ZPI).

[1]To whom correspondence may be addressed. Email: brian.bachmann@vanderbilt.edu or tina.iverson@vanderbilt.edu.

This article contains supporting information online at www.pnas.org/lookup/suppl/doi:10.1073/pnas.1500964112/-/DCSupplemental.

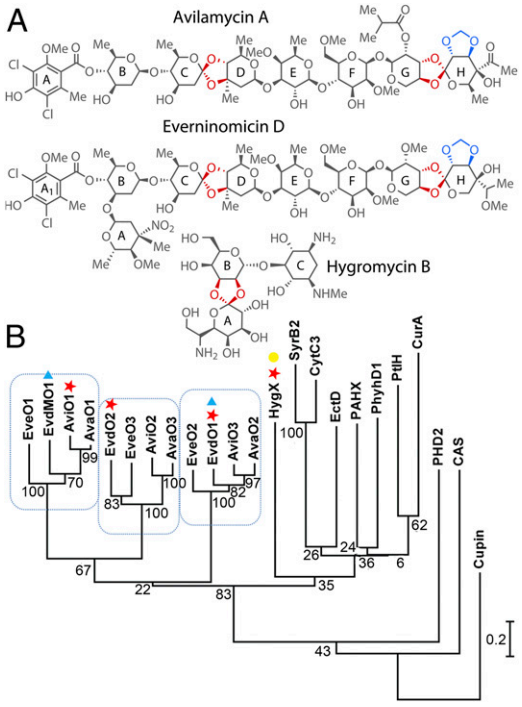

Fig. 1. Orthosomycins and associated oxygenases. (*A*) Orthosomycins with orthoester linkages and methylenedioxy bridges in red. (*B*) Oxygenase phylogenetic analysis. Enzymes characterized structurally (red ★), through gene disruption (blue ▲), and for binding affinity (yellow ●) are indicated.

Results

Comparative Genomic Analysis of AKG/Fe(II)-Dependent Oxygenases. Our studies use five orthosomycin biosynthetic gene clusters available in GenBank: *ava* (avilamycin biosynthesis from *Streptomyces mobaraensis*), *avi* (avilamycin biosynthesis from *S. viridochromogenes Tü57*) (10), *evd* (everninomicin biosynthesis from *Micromonospora carbonacea* var. *aurantiaca*), *eve* (everninomicin biosynthesis from *M. carbonacea* var. *africana*), and *hyg* (hygromycin B biosynthesis from *S. hygroscopicus*). Of these, only the *avi* and *hyg* gene clusters include functional annotation. We therefore used comparative genomics to propose functions for the *ava*, *evd*, and *eve* clusters (Fig. S1). Each cluster contains ORFs encoding enzymes expected in oligosaccharide production, including putative glycosyltransferases, aminotransferases, sugar synthases, and sugar dehydrogenases. Of particular interest are 13 ORFs encoding putative AKG/Fe(II)-dependent oxygenases: three in each of the *ava*, *avi*, *evd*, and *eve* gene clusters and one in the *hyg* gene cluster. The number of putative oxygenases correlates with how many anticipated oxidative cyclizations are required for orthoester linkage and methylenedioxy bridge formation in each antibiotic. Furthermore, these are the only enzymes within each gene cluster that appear to have sufficient catalytic capacity for such oxidations.

Phylogeny of AKG/Fe(II) Oxygenases of Orthosomycin Biosynthesis. Phylogenetic analysis of the 13 putative AKG/Fe(II)-dependent oxygenases of avilamycin, everninomicin, and hygromycin B biosynthesis demonstrates that these enzymes form a distinct subfamily that contains the 13 oxygenases studied here as well as several as-yet-uncharacterized close homologs (a subset is included in Fig. S1). This orthosomycin-associated subfamily is most closely related to the phytanoyl-CoA 2-hydroxylase (PhyH) subfamily of AKG/Fe(II) oxygenases (16–19). Our analysis further separates the orthosomycin-associated oxygenases into subgroups (Fig. 1*B*). The first three subgroups contain one oxygenase from each avilamycin and everninomicin gene cluster, whereas the fourth subgroup contains only HygX. Sequence identity between enzymes of different subgroups is 12–40%, which is consistent with action on distinct substrates. Enzymes belonging to the same subgroup exhibit sequence identities of 70–94%, suggesting that they catalyze the same reaction on either closely related or identical substrates (20). Sequence identities in this range further suggest that an enzyme can represent a subgroup.

Structures of *S. viridochromogenes* AviO1, *M. carbonacea* EvdO1 and EvdO2, and *S. hygroscopicus* HygX Oxygenases. We determined crystal structures for a representative of each phylogenetic subgroup (Fig. 2*A*, Fig. S2 *A–C*, and Tables S1 and S2). Each enzyme adopts the double stranded β-helix motif with the active site housing a metallocenter between β-sheets containing antiparallel β-strands. Despite conservation of fold, the oligomerization state varies, with AviO1 and EvdO2 monomers, EvdO1 a dimer, and HygX a tetramer. Structural similarity searches support our sequence analysis suggesting that the orthosomycin-associated oxygenases are related to the PhyH subfamily of AKG/Fe(II)-dependent oxygenases (16–19). Of note, the halogenases SyrB2 and CytC3 cluster near the orthosomycin-associated oxygenases (13, 21).

Origins of Substrate Specificity. Loop insertions between β-strands of the double stranded β-helix of AKG/Fe(II)-dependent oxygenases are proposed to control substrate specificity (22) and AviO1, EvdO1, EvdO2, and HygX all contain loop inserts to form large binding clefts (Fig. 2*C*, Fig. S2 *D–F*, and Movies S1–S4). Three notable insertions are located at the N- and C-termini and between β-strand IV and β-strand V of the β-helix (Fig. 2*B* and Fig. S2 *D–I*), common sites for specificity-inducing insertions. Smaller inserts in the core fold complement these major insertions.

All insertions have high crystallographic temperature factors, a statistic commonly interpreted as a metric of flexibility. Here, it suggests that substrate binding loops may change conformation upon substrate association. Analysis of the multiple copies of EvdO1 and the HygX in the crystallographic asymmetric units further supports flexibility of these inserts. Four dimers (eight protomers) are located in the EvdO1 asymmetric unit, and these have an average rms deviation of 0.21 Å for the two β-sheets of the double stranded β-helix but an rms deviation of 0.36 Å for the three long loop insertions. Two short loop insertions connecting the outermost β-strands of the double stranded β-helix (approximately residues 129–138 and 226–230) are disordered in four copies. Another striking conformational difference is observed by comparing loops of the four protomers of the HygX-AKG costructure (Fig. 2*D*) to suggest a movement of nearly 20 Å to promote active site closure. Upon hygromycin B binding, the loop adopts the fully closed conformation in all four chains. Conversely, succinate binding results in all four protomers adopting the most open ordered conformation.

Active Site. Our structural studies exploited catalytically inactive Ni^{2+}-substituted enzymes to minimize oxidative damage to the enzyme. This strategy has been used with great success in investigations of Fe(II)/AKG-dependent oxygenases, for example, in the histone demethylases (23–25). Other work has demonstrated that metal substitution does not alter the coordination within the error of crystallographic resolution (26). Metal coordination in canonical AKG/Fe(II)-dependent oxygenases involves two histidines and one acidic residue to form a conserved H-X-D/E. . .H motif known as the facial triad. Whereas AviO1, EvdO1, and EvdO2 retain the facial triad and the Ni^{2+} retains the octahedral coordination geometry typical of iron coordination in the orthosomycin associated AKG/Fe(II)-dependent oxygenases (Fig. S3 *A–C*), HygX exhibits an unexpected variation (Fig. 2 *E* and *F*). We ensured that this variation was not an artifact of

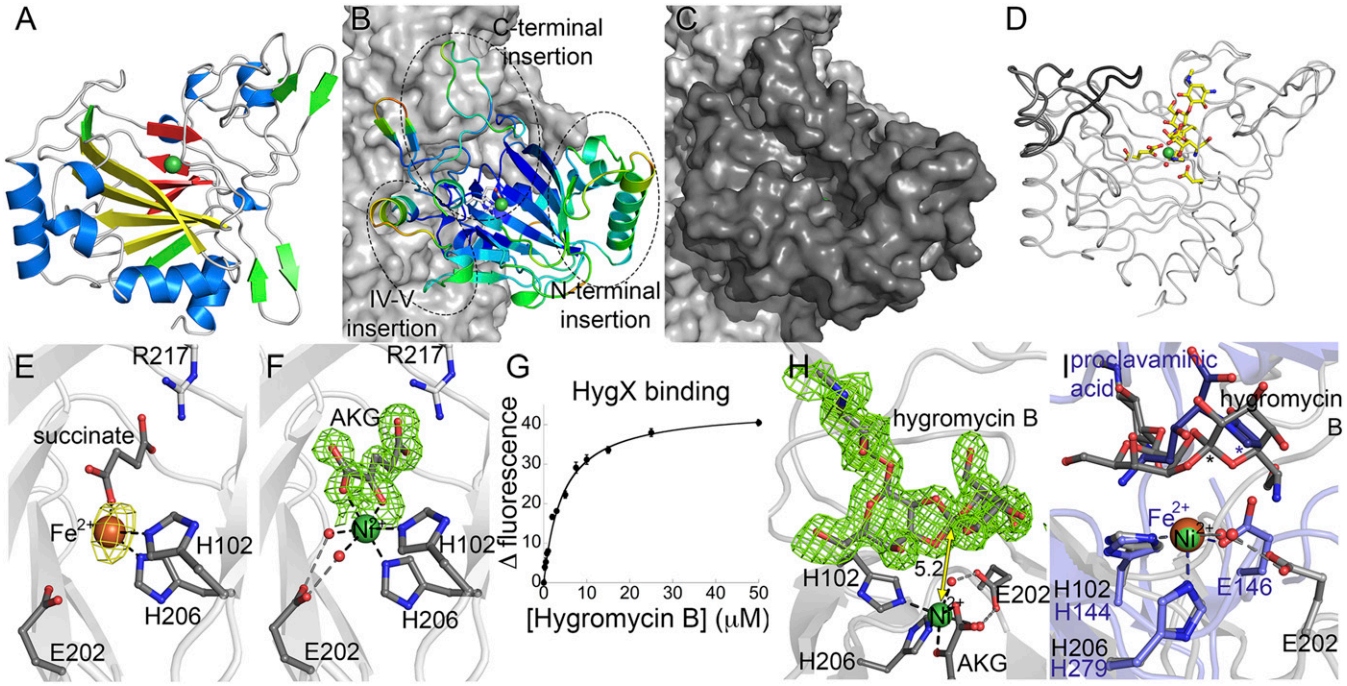

Fig. 2. HygX structure. (*A*) HygX with major strands in yellow and minor strands in red. $Ni^{2+}$and Fe^{2+} are green and orange spheres. (*B*) HygX A chain colored by crystallographic temperature factors where cool colors indicate low B-factors. Loop insertions are highlighted. (*C*) Surface representation in the same orientation as *B*. (*D*) Superposition of four chains of the HygX-AKG complex showing loop movement, with hygromycin B shown for reference. (*E*) Iron coordination with anomalous difference density in yellow and contoured at 5σ. (*F*) Active site metal coordination of HygX. $|F_O| - |F_C|$ difference density is contoured around AKG at 2.5 σ, calculated before inclusion of AKG in the model. (*G*) Tryptophan fluorescence at 350 nm of 0.5 μM HygX, 0.05 mM $NiCl_2$, 0.05 mM AKG, and varying concentrations of hygromycin B (K_d, 3.4 ± 0.5 μM). (*H*) 3σ $|F_O| - |F_C|$ difference density calculated before hygromycin B placement. One possible site of hydrogen atom abstraction is 5.2 Å from the metal center. (*I*) HygX–AKG–hygromycin B product complex (in gray) aligned with the clavaminate synthase–AKG–proclavaminate substrate complex (blue; PDB ID code 1DRT). Asterisks mark sites of hydrogen atom abstraction.

metal substitution by determining the crystal structure of both HygX incorporated with Fe^{2+} and apo-HygX. We observed no significant change in the positions of the coordinating ligands associated with either the change in metal identity or the removal of the metal completely (Fig. 2*E* and Fig. S4). In this variation, the acidic residue of the H-X-D/E. . .H motif is substituted with a glycine, and a glutamic acid located four residues before the distal histidine completes the metal coordination sphere with either a long hydrogen bond or via water-mediated interactions to form a novel H-X-G. . .E-X_3-H motif. The acidic ligand is absent in the halogenases (13, 21), with substrate halides replacing the protein-associated ligand. However, relocation of the acidic ligand is unprecedented.

We determined costructures of these enzymes with AKG or succinate. Clear electron density appeared in the costructures of AKG with EvdO2 and HygX (Fig. 2*F* and Fig. S3*D*). AKG binding is accompanied by slight movements in many of the directly interacting side chains, and a large rotamer change of a conserved arginine (Arg226 of EvdO2 and Arg217 of HygX). As anticipated, the AKG binds directly to the metal center to replace two metal-coordinating solvent molecules in each complex with the 2-keto group *trans* to the acidic residue. Variability in the 1-oxo group coordination has been observed in other AKG/Fe(II)-dependent enzymes, which can be *trans* to either histidine residue (27). In EvdO2, the 1-oxo group is *trans* to the proximal histidine, whereas in HygX, the 1-oxo group is *trans* to the distal histidine. Following crystallization of HygX in 0.6 M succinate, weak electron density is observed for the 1- and 4-carboxylate groups in two of the four protomers. This may reflect the low affinity of succinate in the absence of prime substrate.

HygX Interactions with Hygromycin B. The presence of two putative glycosyltransferases in the *hyg* gene cluster when hygromycin B contains one glycosidic linkage and one orthoester linkage suggests HygX may act upon a substrate with two glycosidic linkages. However, the precise substrate and its stereochemistry are unknown. Because the synthesis of a library of possible substrates is impractical, we assessed whether HygX catalyzed the terminal step of hygromycin B biosynthesis. As enzymes have affinity for their products, we measured HygX binding to hygromycin B using tryptophan fluorescence quenching (K_d, 3.4 ± 0.5 μM; Fig. 2*G*). A low-micromolar affinity is consistent with affinities observed between enzyme and product (28), suggesting HygX catalyzes the last step in hygromycin B biosynthesis. We also determined the costructure of HygX with AKG and hygromycin B to 1.6-Å resolution. Unambiguous electron density for hygromycin B showed a bridging oxygen approaching the metal center (Fig. 2*H*). The binding is highly specific, with the position stabilized by 10 direct and 5 water-mediated interactions (Fig. S5*A*) to promote an orientation in which the anomeric carbon of the destomic acid is 5.2 Å from the metal and 39° from the vertical position of an octahedrally coordinated metal.

Structural comparisons of the HygX–hygromycin B costructure with the EvdO1, EvdO2, and AviO1 structures show that the hygromycin B ligand geometry would result in a steric clash if HygX used a canonical facial triad (Fig. S5). Facial triad modification in HygX both alleviates this steric clash and results in an increased volume of the prime substrate binding pocket. This facial triad is almost invariant across the family; the only known exception is replacement of the acidic residue with a halide substrate in halogenases (13, 21). The likelihood of AviO1, EvdO1, and EvdO2 performing chemical reactions similar to that catalyzed by HygX argues against the novel metal

coordination tuning chemical reactivity toward oxidative ring closure. Instead, modification of the facial triad residues may have arisen solely for substrate accommodation.

Computational Analysis of Disaccharide Interactions with Orthosomycin-Associated Oxygenases. Gene-disruption experiments of oxygenases in *M. carbonacea* var. *aurantiaca* have not as yet produced detectable accumulation of pathway intermediates that would be genuine substrates of these oxygenases. Furthermore, attempts to obtain substrate analogs via synthesis (everninomicin) or reduction (hygromycin B) were unsuccessful. However, the state of the art in computational methods has proven successful at discovering viable binding poses of known ligands (29, 30). Thus, we used two complementary in silico methods and our AviO1, EvdO1, and EvdO2 structures to explore whether productive binding modes of relevant ligands are plausible. We simplified docking calculations by using disaccharide mimics of products for two reasons. First, the carbohydrate chain lengths of the physiologically relevant substrates are unknown, but each product must contain at least two carbohydrates. Second, longer oligosaccharides have many degrees of conformational freedom that would dramatically increase the required search space for docking, reducing the confidence in the results. In contrast, the relative orientation of two sugars constrained by a rigidifying orthoester linkage removes uncertainty from the calculations.

We benchmarked our calculations by docking a talose-destomic acid disaccharide into the HygX structure determined without hygromycin B. The top-scoring binding poses reproduced the experimentally determined position with an rms deviation of 0.70 Å for all atoms and 0.34 Å for the five atoms of the trioxaspiro group. We then docked the C/D and G/H rings of avilamycin and everninomicin with AviO1, EvdO1, and EvdO2. In all cases, at least one pose oriented a disaccharide such that one oxygen atom of the orthoester linkage faces the metal center (Fig. S3 *E–G*). For EvdO1, in particular, the top pose oriented the G/H rings of everninomicin in a manner consistent with methylenedioxy bridge formation (Fig. S3*F*). In multiple instances, we observed clusters of highly related poses representing between 25–50% of the reported hits that were consistent with either orthoesterification or methylenedioxy bridge formation. These calculations suggest that the active site pockets can accommodate substrates in orientations consistent with orthoester linkage formation.

Everninomicin Congeners of *M. carbonacea* var. *aurantiaca*. *M. carbonacea* var. *africana* produces fourteen previously described everninomicin congeners (31–34). Before genetic manipulation, we assessed which everninomicin congeners are produced by *M. carbonacea* var. *aurantiaca* because these have not been reported in the literature. We performed liquid chromatography–MS (LC/MS) analysis of crude extracts followed by tandem LC/MS. This analysis identified four congeners, everninomicins D–G, that vary in the oxidation state of the nitrogen group (-NH_2, -NHOH, -NO, or NO_2) decorating the A-ring (Fig. 3*A*, red, and Fig. S6). The structure of everninomicin E, the amino progenitor to the more oxidized species F and G, was confirmed by high resolution Fourier transform ion cyclotron resonance (FT-ICR) mass spectrometric analysis. Fragmentation (MS^2) provided unambiguous constitutional analysis for the monosaccharide substituents (Fig. 3*B* and Fig. S7), and the expected amine oxidation ladder products corresponding to everninomicins F–G were observed. Of note, everninomicins E, F, and G have not been previously reported.

Targeted Gene Disruption in *M. carbonacea* var. *aurantiaca*. We probed the functions of the *evdO1* and *evdMO1* genes in the production of these congeners by targeted gene disruption. Our approach used modified two-step PCR targeting based on the

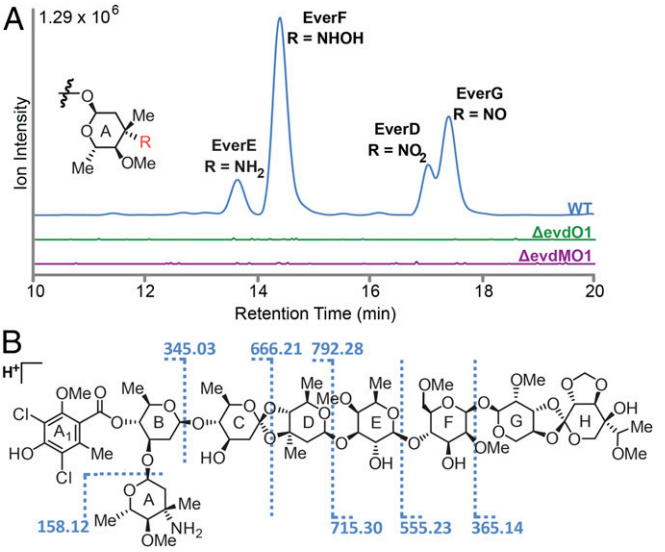

Fig. 3. Oxygenases within the *evd* gene cluster are required for everninomicin production. (*A*) LC/MS of wild-type and deletion strains of *M. carbonacea* var. *aurantiaca* crude extracts. The chromatogram shows summed ion intensities in negative mode for everninomicins D–G: D, *m/z* = 1,534.5 $[M-H]^-$; E, *m/z* = 1,504.5 $[M-H]^-$; F, *m/z* = 1,520.5 $[M-H]^-$; and G, *m/z* = 1,518.5 $[M-H]^-$. No evidence of abundant accumulated metabolites related to everninomicin was observed. Spectra are in Fig. S6. (*B*) FT-ICR-MS^2 of everninomicin E: *m/z* = 1,506.571 $[M+H]^+$. Dashed lines indicate positions of cleavage and masses observed during fragmentation. Spectra are in Fig. S7.

λ-Red recombination system followed by intergeneric conjugation with *Escherichia coli* to transfer plasmid DNA from donor *E. coli* (35). Genetic manipulation in actinomycetes is not well developed, and lack of sporulation by *M. carbonacea* renders conjugation difficult in this organism (36, 37). Thus, we adapted our conjugation method to transform mycelia. A second complication is *M. carbonacea* sensitivity to nalidixic acid, the counterselection marker commonly used to remove donor *E. coli* following conjugation. Thus, we titered the nalidixic acid to stunt the growth of *E. coli*, affording the slower-growing *M. carbonacea* time and space to grow. We then determined that each disruption resulted from a double crossover event using both PCR analysis and Southern hybridization (Fig. S8 and Table S3). LC/MS analysis of crude extracts from the Δ*evdO1* and Δ*evdMO1* strains revealed loss of measurable production of all everninomicin congeners (Fig. 3*A*), with no measurable accumulation of mass features readily identifiable as everninomicin biosynthetic intermediates. The loss of everninomicin production confirms the importance of oxygenase activity in everninomicin biosynthesis.

Discussion

Substrate Identity and Selectivity. Genomic analysis, gene disruption, and structural characterization with ligands can suggest function for natural product biosynthetic enzymes (15, 38, 39), and our data strongly support a role for HygX in catalyzing orthoester linkage formation. Together, these data suggest a fully decorated three-ringed compound lacking the orthoester linkage as the substrate and narrows the possibilities for HygX substrates to two alternative anomers at C1 of the destomic acid moiety. The lack of readily available potential precursor molecules renders chemical synthesis of either of these anomers enormously challenging.

Reasonable sequence identities between HygX and each of the remaining 12 AKG/Fe(II)-dependent oxygenases in everninomicin and avilamycin biosynthesis suggest roles for the latter enzymes in carbohydrate-associated oxidative ring closures.

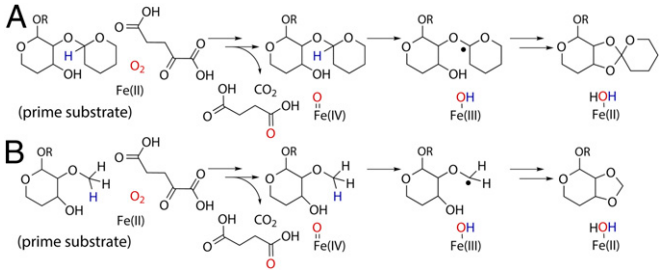

Fig. 4. Mechanistic possibilities for orthosomycin-associated oxygenases. Generation of the Fe(IV)=O species is conserved within the superfamily and not shown. (*A*) The first step of orthoester linkage formation may be radical generation by hydrogen atom abstraction, as suggested by structural parallels with clavaminate synthase catalyzed oxidative ring closure. The regiochemistry of the preexisting glycosidic bond is not known. (*B*) Methylenedioxy bridge formation may also use hydrogen atom abstraction by the Fe(IV)=O species. The position of the methoxy group at C2 or C3 is unknown.

Previous experimental assessment of the function of orthosomycin-associated oxygenases is limited to gene disruption of *aviO1*, *aviO2*, and *aviO3* of avilamycin biosynthesis. Deletion of *aviO2* (*evdO2* homolog) from *S. viridochromogenes Tü57* resulted in a new peak in the mass spectrum, interpreted as the loss of the acetyl group on C4 of the H-ring (see Fig. 1*A* for location) (40). Given that an AKG/Fe(II)-dependent oxygenase is unlikely to catalyze acetylation and that the homologous oxygenase is present in the *evd* and *eve* gene clusters despite the absence of an acetyl group on everninomicin congeners, an alternative interpretation of this result is that AviO2 catalyzes a ring closure before acetylation and that this ring closure is required for substrate recognition by an acetylating enzyme. Consistent with this interpretation, our computational studies suggest that the homolog EvdO2 can reasonably orient the G/H rings.

The assignment of function to the remaining enzymes is more tenuous. Deletion of both *aviO1* (*evdMO1* homolog) and *aviO3* (*evdO1* homolog) from *S. viridochromogenes Tü57* resulted in loss of detectable avilamycin production (40), mirroring our results of loss of detectable everninomicin production upon the deletion of *evdO1* and *evdMO1*. The lack of any detectable species precludes assignment of precise catalytic function.

Preliminary Reaction Scheme. All characterized AKG/Fe(II)-dependent oxygenases have conserved aspects to their reaction cycle. For example, these powerful oxidants function via two sequential half reactions that require sequential binding of three substrates: AKG, prime substrate, and O_2. The first half-reaction converts the cosubstrate AKG to succinate, whereas the second half-reaction converts prime substrate to product. A combination of kinetic, biochemical, and structural studies support a unified mechanism for cosubstrate catalysis that generates the highly reactive Fe(IV)= O oxidizing species (41–44).

Numerous schemes for prime substrate catalysis are observed in the superfamily. The most relevant to orthoester linkage and methylenedioxy bridge formation is oxidative cyclization by clavaminate synthase, where hydrogen atom abstraction from substrate (45) is followed by ring closure. Comparison of hygromycin B in the HygX costructure to that of the proclavaminic acid substrate bound to clavaminate synthase (14) aligns an anomeric carbon of hygromycin B with the carbon atom of proclavaminate that undergoes hydrogen atom abstraction (Fig. 2*I*). This carbon atom is 5.4 Å from the metal in the clavaminate synthase–proclavaminate costructure and 5.2 Å in the HygX–hygromycin B costructure. The C1 carbon of the hygromycin B precursor is one logical site for hydrogen atom abstraction (Fig. 4*A*), although alternative positions, such as the hydroxyl group, cannot be excluded (46). Analogous abstraction possibilities exist to initiate methylenedioxy bridge formation (Fig. 4*B*).

In the context of this reaction scheme, several possible mechanisms could support orthoester linkage and methylenedioxy bridge formation following initial hydrogen atom abstraction. Options include oxidative radical coupling (with or without ligand transfer or oxygen rebound), nucleophilic capture of an oxocarbenium ion, or a ketene acetal intermediate (47). Because P450 enzymes are the only characterized enzymes that catalyze methylenedioxy bridge formation, we examined that mechanism closely. The paucity of P450 enzymes that can act as pure dehydrogenases resulted in a proposal of Fe-centered radical chemistry with an oxygen rebound mechanism followed by water elimination from the hydroxylated intermediate (48). Oxygen rebound leading to hydroxylation and elimination on a C2/C3 methoxy of the H-rings is supported by the AKG/Fe(II)-dependent superfamily scaffold. However, AKG/Fe(II)-dependent enzymes can also catalyze dehydrogenation of a C2/C3 methoxy group without ligand insertion and/or oxygen rebound, which could allow for methylenedioxy formation by quenching an oxonium intermediate. Other possible mechanisms for methylenedioxy formation are possible. For instance, in the event of a C2-deoxy H-ring precursor, C2 oxygenation and sequential oxidative desaturation circumvents the oxonium intermediate.

Potential for Engineering Altered Reactivity into AKG/Fe(II)-Dependent Enzymes. Whereas Ziracin stalled in phase III clinical trials, everninomicin analogs still hold promise for clinical use. Everninomicin synthesis is challenging (49), likely making de novo production of analogs prohibitively expensive, but analogs could be produced by engineering the biosynthetic enzymes in the producing organism. The loss of detectable everninomicin production for the Δ*evdO1* and Δ*evdMO1* strains indicates that functional oxygenase activity is critical for everninomicin production. Thus, any bioengineering requires that substrate selectivity of the AKG/Fe(II)-dependent oxygenases be modified.

Within the AKG/Fe(II)-dependent superfamily, the halogenases are among the more closely related to the orthosomycin associated oxygenases. Excepting HygX, these are the only enzymes with a modified metal-coordinating facial triad. Interestingly, the ability of the AKG/Fe(II)-dependent halogenase SyrB2 to catalyze halogenation or hydroxylation is influenced by subtle changes to either the halide binding site or the substrate (50) and can be tuned to catalyze unnatural reactions, such as nitration of unactivated carbon centers (51). Interestingly, sequence-similarity searches using the 13 enzymes studied here also identify as-yet-uncharacterized very close homologs (a subset is listed in Fig. S1), which presents an opportunity to explore further reactions catalyzed by the oxygenase superfamily and investigate the capability of these oxygenases to accept expanded substrates.

Materials and Methods

Protocols for gene cloning, protein overexpression, purification, crystallization, data collection, structure determination and refinement, gene disruption, and mass spectral analysis are available in *SI Materials and Methods*.

ACKNOWLEDGMENTS. We thank Dr. Jeffrey Spraggins of the Vanderbilt Mass Spectrometry Research Center for help with the Fourier transform ion cyclotron resonance mass spectrometric analysis of everninomicin E. This work was supported by National Institutes of Health (NIH) Grant T32 HL007751 (to K.M.M.), the Vanderbilt Summer Science Academy (J.L.M.), the Vanderbilt Institute of Chemical Biology (B.O.B.), Office of Naval Research Grant N00014-09-1-012 (to B.O.B.), and American Heart Association Grant 12GRNT11920011 (to T.M.I.). The Vanderbilt crystallization facility was supported by NIH Grant S10 RR026915. Use of the Advanced Photon Source, an Office of Science User Facility operated for the US Department of Energy (DOE) Office of Science by Argonne National Laboratory, was supported by the US DOE under Contract DE-AC02-06CH11357. Use of the LS-CAT Sector 21 was supported by the Michigan Economic Development Corporation and the Michigan Technology Tri-Corridor (Grant 085P1000817).

BIOCHEMISTRY

1. Fischbach MA, Walsh CT (2009) Antibiotics for emerging pathogens. *Science* 325(5944):1089–1093.
2. Jones RN, Low DE, Pfaller MA (1999) Epidemiologic trends in nosocomial and community-acquired infections due to antibiotic-resistant gram-positive bacteria: The role of streptogramins and other newer compounds. *Diagn Microbiol Infect Dis* 33(2): 101–112.
3. Adrian PV, et al. (2000) Evernimicin (SCH27899) inhibits a novel ribosome target site: Analysis of 23S ribosomal DNA mutants. *Antimicrob Agents Chemother* 44(11):3101–3106.
4. Belova L, Tenson T, Xiong L, McNicholas PM, Mankin AS (2001) A novel site of antibiotic action in the ribosome: Interaction of evernimicin with the large ribosomal subunit. *Proc Natl Acad Sci USA* 98(7):3726–3731.
5. Waitz JA, Horan AC (1988) Micromonospora carbonacea var africana. US Patent 4,735,903.
6. Mann RL, Bromer WW (1958) The isolation of a second antibiotic from *Streptomyces hygroscopicus*. *J Am Chem Soc* 80(11):2714–2716.
7. Díaz Chávez ML, Rolf M, Gesell A, Kutchan TM (2011) Characterization of two methylenedioxy bridge-forming cytochrome P450-dependent enzymes of alkaloid formation in the Mexican prickly poppy *Argemone mexicana*. *Arch Biochem Biophys* 507(1):186–193.
8. Ikezawa N, et al. (2003) Molecular cloning and characterization of CYP719, a methylenedioxy bridge-forming enzyme that belongs to a novel P450 family, from cultured *Coptis japonica* cells. *J Biol Chem* 278(40):38557–38565.
9. Hofmann C, et al. (2005) Genes encoding enzymes responsible for biosynthesis of L-lyxose and attachment of eurekanate during avilamycin biosynthesis. *Chem Biol* 12(10):1137–1143.
10. Weitnauer G, et al. (2001) Biosynthesis of the orthosomycin antibiotic avilamycin A: Reductions from the molecular analysis of the *avi* biosynthetic gene cluster of *Streptomyces viridochromogenes Tü57* and production of new antibiotics. *Chem Biol* 8(6):569–581.
11. Wang C, et al. (2013) Evidence that the fosfomycin-producing epoxidase, HppE, is a non-heme-iron peroxidase. *Science* 342(6161):991–995.
12. Strieker M, Kopp F, Mahlert C, Essen LO, Marahiel MA (2007) Mechanistic and structural basis of stereospecific Cbeta-hydroxylation in calcium-dependent antibiotic, a daptomycin-type lipopeptide. *ACS Chem Biol* 2(3):187–196.
13. Blasiak LC, Vaillancourt FH, Walsh CT, Drennan CL (2006) Crystal structure of the non-haem iron halogenase SyrB2 in syringomycin biosynthesis. *Nature* 440(7082):368–371.
14. Zhang Z, et al. (2000) Structural origins of the selectivity of the trifunctional oxygenase clavaminic acid synthase. *Nat Struct Biol* 7(2):127–133.
15. Zhao S, et al. (2013) Discovery of new enzymes and metabolic pathways by using structure and genome context. *Nature* 502(7473):698–702.
16. Reuter K, et al. (2010) Synthesis of 5-hydroxyectoine from ectoine: Crystal structure of the non-heme iron(II) and 2-oxoglutarate-dependent dioxygenase EctD. *PLoS One* 5(5):e10647.
17. Khare D, et al. (2010) Conformational switch triggered by α-ketoglutarate in a halogenase of curacin A biosynthesis. *Proc Natl Acad Sci USA* 107(32):14099–14104.
18. You Z, Omura S, Ikeda H, Cane DE, Jogl G (2007) Crystal structure of the non-heme iron dioxygenase PtlH in pentalenolactone biosynthesis. *J Biol Chem* 282(50): 36552–36560.
19. McDonough MA, et al. (2005) Structure of human phytanoyl-CoA 2-hydroxylase identifies molecular mechanisms of Refsum disease. *J Biol Chem* 280(49): 41101–41110.
20. Tian W, Skolnick J (2003) How well is enzyme function conserved as a function of pairwise sequence identity? *J Mol Biol* 333(4):863–882.
21. Wong C, Fujimori DG, Walsh CT, Drennan CL (2009) Structural analysis of an open active site conformation of nonheme iron halogenase CytC3. *J Am Chem Soc* 131(13): 4872–4879.
22. Aik W, McDonough MA, Thalhammer A, Chowdhury R, Schofield CJ (2012) Role of the jelly-roll fold in substrate binding by 2-oxoglutarate oxygenases. *Curr Opin Struct Biol* 22(6):691–700.
23. Chowdhury R, et al. (2014) Ribosomal oxygenases are structurally conserved from prokaryotes to humans. *Nature* 510(7505):422–426.
24. Krishnan S, Trievel RC (2013) Structural and functional analysis of JMJD2D reveals molecular basis for site-specific demethylation among JMJD2 demethylases. *Structure* 21(1):98–108.
25. Couture J-F, Collazo E, Ortiz-Tello PA, Brunzelle JS, Trievel RC (2007) Specificity and mechanism of JMJD2A, a trimethyllysine-specific histone demethylase. *Nat Struct Mol Biol* 14(8):689–695.
26. Horton JR, Upadhyay AK, Hashimoto H, Zhang X, Cheng X (2011) Structural basis for human PHF2 Jumonji domain interaction with metal ions. *J Mol Biol* 406(1):1–8.
27. Zhang Z, et al. (2002) Crystal structure of a clavaminate synthase-Fe(II)-2-oxoglutarate-substrate-NO complex: Evidence for metal centered rearrangements. *FEBS Lett* 517(1-3):7–12.
28. Bar-Even A, et al. (2011) The moderately efficient enzyme: Evolutionary and physicochemical trends shaping enzyme parameters. *Biochemistry* 50(21):4402–4410.
29. Isin B, Estiu G, Wiest O, Oltvai ZN (2012) Identifying ligand binding conformations of the β2-adrenergic receptor by using its agonists as computational probes. *PLoS One* 7(12):e50186.
30. Singh PK, et al. (2013) Plasticity of the quinone-binding site of the complex II homolog quinol:fumarate reductase. *J Biol Chem* 288(34):24293–24301.
31. Ganguly AK, Sarre OZ, Greeves D, Morton J (1975) Letter: Structure of everninomicin D-1. *J Am Chem Soc* 97(7):1982–1985.
32. Wright DE (1979) The Orthosomycins, a new family of antibiotics. *Tetrahedron* 35: 1207–1237.
33. Ganguly AK, et al. (1989) The structure of new oligosaccharide antibiotics, 13-384 components 1 and 5. *Heterocycles* 28(1):83–88.
34. Chu M, et al. (2002) Isolation and characterization of novel oligosaccharides related to Ziracin. *J Nat Prod* 65(11):1588–1593.
35. Gust B, Challis GL, Fowler K, Kieser T, Chater KF (2003) PCR-targeted *Streptomyces* gene replacement identifies a protein domain needed for biosynthesis of the sesquiterpene soil odor geosmin. *Proc Natl Acad Sci USA* 100(4):1541–1546.
36. Hosted TJ, Wang TX, Alexander DC, Horan AC (2001) Characterization of the biosynthetic gene cluster for the oligosaccharide antibiotic, Evernimicin, in *Micromonospora carbonacea* var. *africana* ATCC39149. *J Ind Microbiol Biotechnol* 27(6):386–392.
37. Flett F, Mersinias V, Smith CP (1997) High efficiency intergeneric conjugal transfer of plasmid DNA from Escherichia coli to methyl DNA-restricting streptomycetes. *FEMS Microbiol Lett* 155(2):223–229.
38. Singh S, Nandurkar NS, Thorson JS (2014) Characterization of the calicheamicin orsellinate C2-O-methyltransferase CalO6. *ChemBioChem* 15(10):1418–1421.
39. McCoy JG, et al. (2009) Structural characterization of CalO2: A putative orsellinic acid P450 oxidase in the calicheamicin biosynthetic pathway. *Proteins* 74(1):50–60.
40. Treede I, et al. (2005) Genes involved in formation and attachment of a two-carbon chain as a component of eurekanate, a branched-chain sugar moiety of avilamycin A. *Appl Environ Microbiol* 71(1):400–406.
41. Price JC, Barr EW, Glass TE, Krebs C, Bollinger JM, Jr (2003) Evidence for hydrogen abstraction from C1 of taurine by the high-spin Fe(IV) intermediate detected during oxygen activation by taurine:α-ketoglutarate dioxygenase (TauD). *J Am Chem Soc* 125(43):13008–13009.
42. Price JC, Barr EW, Tirupati B, Bollinger JM, Jr, Krebs C (2003) The first direct characterization of a high-valent iron intermediate in the reaction of an α-ketoglutarate-dependent dioxygenase: A high-spin FeIV complex in taurine/α-ketoglutarate dioxygenase (TauD) from Escherichia coli. *Biochemistry* 42(24):7497–7508.
43. Proshlyakov DA, Henshaw TF, Monterosso GR, Ryle MJ, Hausinger RP (2004) Direct detection of oxygen intermediates in the non-heme Fe enzyme taurine/α-ketoglutarate dioxygenase. *J Am Chem Soc* 126(4):1022–1023.
44. Riggs-Gelasco PJ, et al. (2004) EXAFS spectroscopic evidence for an Fe=O unit in the Fe (IV) intermediate observed during oxygen activation by taurine:α-ketoglutarate dioxygenase. *J Am Chem Soc* 126(26):8108–8109.
45. Iwata-Reuyl D, Basak A, Townsend CA (1999) β-Secondary kinetic isotope effects in the clavaminate synthase-catalyzed oxidative cyclization of proclavaminic acid and in related azetidinone model reactions. *J Am Chem Soc* 121(49):11356–11368.
46. Borowski T, de Marothy S, Broclawik E, Schofield CJ, Siegbahn PEM (2007) Mechanism for cyclization reaction by clavaminic acid synthase. Insights from modeling studies. *Biochemistry* 46(12):3682–3691.
47. Beau J-M, Jaurand G, Esnault J, Sinaÿ P (1987) Synthesis of the disaccharide C•D fragment found in everninomicin-C and -D, avalamycin-A and -C and curamycin-A: Stereochemistry at the spiro-ortholactone center. *Tetrahedron Lett* 28(10):1105–1108.
48. Bjorklund JA, et al. (1995) Cryptic stereochemistry of berberine alkaloid biosynthesis. *J Am Chem Soc* 117(5):1533–1545.
49. Nicolaou KC, et al. (2000) Total synthesis of everninomicin 13,384-1–Part 1: Retrosynthetic analysis and synthesis of the A1B(A)C fragment. *Chemistry* 6(17):3095–3115.
50. Matthews ML, et al. (2009) Substrate positioning controls the partition between halogenation and hydroxylation in the aliphatic halogenase, SyrB2. *Proc Natl Acad Sci USA* 106(42):17723–17728.
51. Matthews ML, et al. (2014) Direct nitration and azidation of aliphatic carbons by an iron-dependent halogenase. *Nat Chem Biol* 10(3):209–215.
52. Otwinowski Z, Minor W (1997) Processing of X-ray diffraction data collected in oscillation mode. *Methods Enzymol* 276:307–326.
53. Sheldrick GM (2010) Experimental phasing with SHELXC/D/E: Combining chain tracing with density modification. *Acta Crystallogr D Biol Crystallogr* 66(Pt 4):479–485.
54. Pape T, Schneider TR (2004) HKL2MAP: A graphical user interface for macromolecular phasing with SHELX programs. *J Appl Cryst* 37(5):843–844.
55. Terwilliger TC, et al. (2009) Decision-making in structure solution using Bayesian estimates of map quality: The PHENIX AutoSol wizard. *Acta Crystallogr D Biol Crystallogr* 65(Pt 6):582–601.
56. Adams PD, et al. (2010) PHENIX: A comprehensive Python-based system for macromolecular structure solution. *Acta Crystallogr D Biol Crystallogr* 66(Pt 2):213–221.
57. McCoy AJ, et al. (2007) *Phaser* crystallographic software. *J Appl Cryst* 40(Pt 4):658–674.
58. Zhang Z, et al. (2011) Crystal structure of PHYHD1A, a 2OG oxygenase related to phytanoyl-CoA hydroxylase. *Biochem Biophys Res Commun* 408(4):553–558.
59. Terwilliger TC, et al. (2008) Iterative model building, structure refinement and density modification with the PHENIX AutoBuild wizard. *Acta Crystallogr D Biol Crystallogr* 64(Pt 1):61–69.
60. Emsley P, Lohkamp B, Scott WG, Cowtan K (2010) Features and development of Coot. *Acta Crystallogr D Biol Crystallogr* 66(Pt 4):486–501.
61. Brunger AT (2007) Version 1.2 of the Crystallography and NMR system. *Nat Protoc* 2(11):2728–2733.
62. Afonine PV, et al. (2012) Towards automated crystallographic structure refinement with *phenix.refine*. *Acta Crystallogr D Biol Crystallogr* 68(Pt 4):352–367.
63. Friesner RA, et al. (2006) Extra precision glide: Docking and scoring incorporating a model of hydrophobic enclosure for protein-ligand complexes. *J Med Chem* 49(21): 6177–6196.
64. Jain AN (2007) Surflex-Dock 2.1: Robust performance from ligand energetic modeling, ring flexibility, and knowledge-based search. *J Comput Aided Mol Des* 21(5): 281–306.
65. Jain AN (1996) Scoring noncovalent protein-ligand interactions: A continuous differentiable function tuned to compute binding affinities. *J Comput Aided Mol Des* 10(5):427–440.